JPET Fast Forward. Published on November 10, 2003 as DOI: 10.1124/jpet.103.060301

JPET #60301

Targeted Disruption of the Olfactory Mucosa-Specific *Cyp2g1* Gene: Impact on Acetaminophen Toxicity in the Lateral Nasal Gland, and Tissue-selective Effects on *Cyp2a5* Expression

XIAOLIANG ZHUO[†], JUN GU, MELISSA J. BEHR, PAM J. SWIATEK,[‡] HUADONG CUI, QING-YU ZHANG, YINGQIU XIE, DORIS N. COLLINS, AND XINXIN DING

Wadsworth Center, New York State Department of Health, and School of Public Health, State University of New York at Albany, NY 12201

Running title: *Cyp2g1*-Null Mice

Address correspondence to:

Dr. Xinxin Ding, Wadsworth Center, New York State Department of Health, Empire State Plaza, Box 509, Albany, NY 12201-0509.

Tel. 518-486-2585; Fax: 518-486-1505; E-mail: xding@wadsworth.org

Number of Text Pages: 25

Number of Tables: 6

Number of Figures: 4

Number of References: 40

Number of words: 245 (Abstract)

560 (Introduction)

1496 (Discussion)

ABBREVIATIONS: CYP, cytochrome P450; CPR, NADPH-cytochrome P450 reductase; BAC, bacterial artificial chromosome; OM, olfactory mucosa; AP, acetaminophen; DCBN, 2,6-dichlorobenzonitrile; PEG, polyethylene glycol; ALT, alanine aminotransferase; *o*-HPA, *o*-hydroxyphenylacetaldehyde; LNG, lateral nasal gland; ES, embryonic stem; kb, kilobase pair; bp, base pair.

SECTION ASSIGNMENT: Toxicology

ABSTRACT

CYP2G1 is a cytochrome P450 monooxygenase expressed uniquely in the olfactory mucosa (OM). We have generated *Cyp2g1*-null mice to identify the roles of CYP2G1 in the biology and the tissue-specific toxicity of xenobiotic compounds in the nose. Homozygous *Cyp2g1*-null mice are viable and fertile; they show no evidence of embryonic lethality, morphological abnormality, or developmental deficits; and they seem to have normal olfactory ability. However, OM microsomes from *Cyp2g1*-null mice were found to have significantly lower activities than microsomes from wild-type mice in the metabolism of testosterone and progesterone (~60% decrease), and in the metabolic activation of coumarin (>70% decrease). Unexpectedly, a significant reduction in the expression of the *Cyp2a5* gene was found in the liver, the lateral nasal gland (LNG), and, to a lesser extent, the kidney of adult *Cyp2g1*-null mice. The loss of CYP2G1 expression, and the associated decrease in the hepatic expression of CYP2A5, did not decrease systemic clearance, extent of hepatotoxicity, or OM toxicity of acetaminophen (AP). However, the LNG was protected from AP (at 400 mg/kg) toxicity in the *Cyp2g1*-null mice. Paradoxically, the LNG did not have detectable CYP2G1, and the decrease in LNG CYP2A5 expression in the *Cyp2g1*-null mice was not accompanied by decreases in microsomal AP metabolism. We hypothesize that OM CYP2G1 (through a paracrine pathway) or LNG CYP2A5 may indirectly influence resistance of the LNG to chemical toxicity, possibly by regulating gene expression in the LNG through steroid hormones or other endogenous CYP substrates and their metabolites.

The tissue-specific expression of CYP2G1 in the OM is highly conserved in mammals (see Ding and Dahl, 2003, for a recent review). CYP2G1 is a major CYP enzyme in OM microsomes of rabbits and mice. *In vitro* metabolic assays with heterologously expressed mouse CYP2G1 or purified rabbit or bovine CYP2G1 revealed high activity with sex steroid hormones, including androstenedione, testosterone, 5α-dihydrotestosterone, progesterone, and estradiol. CYP2G1 is also active toward arachidonic acid, producing both epoxy- and hydroxy-eicosatrienoic acids. In addition, CYP2G1 is active in the metabolism of numerous exogenous compounds, including compounds known to cause tissue-selective toxicity in the nasal mucosa, such as coumarin, DCBN (herbicide), and AP. The substrate specificities, combined with the tissue-selective expression pattern of this enzyme, suggest that CYP2G1 may be critical in target tissue metabolic activation and the consequent cytotoxicity of nasal toxicants, and that it may have important biological functions in the olfactory chemosensory organ through its metabolic activities toward endogenous substrates. These intriguing possibilities were explored in the present study through development and characterization of a *Cyp2g1*-null mouse model.

Unlike many of the multi-gene subfamilies in the mouse *Cyp2* gene family, the *Cyp2g* subfamily contains only a single gene, *Cyp2g1*. The structure of the mouse *Cyp2g1* gene has been characterized; this gene contains nine exons, and the transcriptional initiation sites are located at 16 and 15 base pairs upstream of the translation start codon (Zhuo et al., 2001). The *Cyp2g1* gene is located in a *Cyp2* gene cluster on mouse chromosome 7, next to the *Cyp2a5* gene (Wang et al., 2003). In this study, we have generated *Cyp2g1*-null mice by replacing exon 3 of the *Cyp2g1* gene with the *neo* gene. The homozygous mutant mice were examined for phenotypic abnormalities, including changes in olfactory ability, and to determine the impact of *Cyp2g1* gene disruption on the expression of CYP2G1 and on the activities of OM microsomes

toward a number of known CYP2G1 substrates. Potential compensatory increases in other CYPs, and related enzymes, in the OM and liver were also examined. Furthermore, the impact of *Cyp2g1* knockout on the metabolism and toxicity of AP was determined for OM and LNG (also known as Steno's gland).

The LNG is the largest of about 20 anterior nasal glands that drain by long ducts that open near the nostril in mice and rats; it has been found in most mammalian species, including man (Moe and Bojsen-Moller, 1971). The LNG is the major site for the synthesis and secretion of odorant-binding proteins, which are abundant, soluble, nasal proteins, and are believed to function mainly as carriers for odorants in the nasal mucus (Snyder et al., 1988). In addition, the secretions of the LNG are believed to humidify inspired air (Snyder et al., 1988), and the large amounts of immunoglobulin A in the LNG secretions (Adams et al., 1981) may be important for the immune barrier function of the OM (Getchell and Mellert, 1991). The potential roles of the LNG in olfactory chemoreception, as well as in host defense, make it an important target for chemical toxicity. Indeed, the LNG is a known target for the toxicity of both inhaled (such as divinylbenzene-55 (Morgan et al., 1997)), and systemically administered (such as 4-(methylnitrosamino)-1-(3-pyridyl)-1-butanone (Belinsky et al., 1987)) chemicals, and here we show for the first time that the LNG is a major target for the cytotoxicity of AP in mice.

Materials and Methods

Targeting Vector Construction. The targeting vector (Fig. 1) was prepared in a pGK-neo-tk vector (6.5 kb) provided by the Transgenic and Knockout Core Facility of the Wadsworth Center. It consists of a pBluescript backbone (Stratagene, La Jolla, CA) and, in the same orientation, a PGK-neo-bpA cassette for neo gene expression (Soriano et al., 1991) and the MC1-tk-pA cassette for thymidine kinase gene expression (Mansour et al., 1988). BAC clones containing the mouse *Cyp2g1* gene have been described recently (Zhuo et al., 2001). A 7.2-kb *BamH* I fragment and a 2.0-kb *Hind* III fragment of the *Cyp2g1* gene were inserted into pGK-neo-tk vector at *BamH* I and *Hind* III sites, respectively. The targeting vector containing the inserts with the correct orientation was linearized with *Sal* I, and was concentrated to 1 μg/μl using a Microcon 30 spin column (Amicon, Billerica, MA).

Electroporation and Selection of ES Cells. CJ7 ES cells (Swiatek and Gridley, 1993) at passage 4 were trypsinized and resuspended in PBS at 2 x 10^7 cells/ml. The resuspended cells (0.8 ml) were electroporated with 25 μg of linearized targeting vector DNA using a Bio-Rad gene pulser (500 μF, 240V). Following electroporation, cells were cultured on tissue culture plates containing mitomycin C-treated primary embryonic fibroblast feeder layers prepared from a transgenic mouse line that expresses the *neo* gene (Stewart et al., 1992). After 24 hr, the media were replaced with selection media containing, in addition to routine supplements, G418 (Invitrogen, Carlsbad, CA; 250 μg active ingredient/ml) and Ganciclovir (Syntex, Boulder, Co; 2 μM). Media were changed daily. Colonies were picked individually 6 to 7 days after electroporation, dissociated in trypsin-EDTA, and plated into 48-well culture plates containing the feeder cells. The G418-resistant ES cell colonies in the 48-well dishes were trypsinized, and

50% of the cells were replica plated into new 24-well dishes to grow for DNA isolation. The remaining cells were stored at -80^{o}C for subsequent culture and blastocyst injection.

Genotyping ES Cells and Mice. Genomic PCR was performed with DNA (500 ng for each reaction) isolated from cultured ES cells or mouse tails (Hogan et al. 1994). Primers E2U (5'-ggttgtcttatgtggacatgaggc-3') and NeoL (5'-cacttgtgtagcgccaagtgccag-3'), as shown in Fig. 1, were used to amplify a 550-bp DNA fragment from the targeted allele, whereas primers E2U and E3L (5'-caatcgttctccattggacagagc-3') were used to amplify a 1.6-kb fragment from the wild-type allele. PCR mixtures (25 μl) contained, in addition to genomic DNA and 200 nM of each primer, 1X PCR buffer (Promega, Madison, WI), 2 mM $MgCl_2$, dNTPs (0.5 mM each), and 2 U of Taq DNA polymerase (Promega). The PCR program included 35 cycles of denaturation at 95^{o} C for 45 sec, annealing at 59.5^{o} C for 50 sec, and extension at 72^{o} C for 45 sec.

For Southern blot analysis, genomic DNA was digested overnight with 50 U of *Pst* I (Roche, Indianapolis, IN) at 37^{o} C. The fragments were separated on an agarose gel and hybridized with [α-^{32}P]dCTP-labeled probe H, which was a 1.0-kb *Hind* III fragment from the 5'-flanking sequence external to the targeting vector (Fig. 1). Hybridization was performed in QuikHyb hybridization solution (Stratagene), with salmon sperm DNA, at 58 ^{o}C for 4 hr. Fragments of 6.5 kb and 5.5 kb were expected to represent the wild-type and targeted alleles, respectively.

Blastocyst Injection and Animal Breeding. Recombinant ES cells were trypsinized, centrifuged, and resuspended in injection media (Hogan et al., 1994). Ten to 15 ES cells were injected into the blastocoel cavity of 3.5 dpc blastocysts from C57BL/6J (B6) female mice. The blastocysts were implanted into the uteri of pseudopregnant B6/CBA F1 mice to generate offspring. The male chimeras were bred with wild-type B6 female mice to obtain germline

transmission F1 mice that are heterozygous for the targeted allele. The F2 homozygotes were obtained by intercrossing the F1 heterozygotes.

RNA Blot Analysis. Total RNA was isolated from mouse tissues using TRIzol Reagent (Invitrogen) according to the manufacturer's instructions. For RNA blot analysis, hybridization was carried out overnight, at 58 ^{o}C, in QuikHyb hybridization solution (Stratagene), with an [α-^{32}P]dCTP-labeled full-length mouse *Cyp2g1* cDNA (Hua et al., 1997) or a *Cyp2a5* cDNA (Su et al., 1998).

RNA-PCR. Qualitative PCR detection of CYP1A2, CYP2A5 (Zhang et al., 2003), and CYP2G1 (Gu et al., 1999) transcripts was performed as previously described; the expected products are 359 bp, 318 bp, and 489 bp, respectively. First-strand cDNA was synthesized by reverse transcription from 1 μg of total RNA with use of Moloney Murine Leukemia virus reverse transcriptase (Promega) and a $d(T)_{16}$ primer (Applied Biosystems, Forster City, CA). Real-time PCR was carried out in a LightCycler instrument (Roche), with the PCR mixtures containing 2 μl of FastStart DNA Master SYBR Green I (Roche), 2 mM $MgCl_2$, 0.4 μM of each primer, and 1 μl of a reverse transcription mixture, in a total volume of 20 μl. For quantitation of CYP2A5 mRNA, a pair of CYP2A5-specific primers was used (forward primer: 5'-cctgtattcaccatctacctgggac-3'; reverse primer: 5'-ctccccgctgctgaagactac-3'), which do not amplify CYP2A4 or CYP2A12. The PCR program included 50 cycles of denaturation at 95 ^{o}C for 2 sec, annealing at 60 ^{o}C for 5 sec, and extension at 72 ^{o}C for 25 sec. CYP2F2 (forward primer: 5'-ggataccaaactgtgaaggaggctc-3'; reverse primer: 5'-ccaggtatccaatcaaggacacttgg-3'; denaturation for 5 sec, annealing at 62 ^{o}C, and extension for 30 sec) and β-actin (forward primer: 5'-acccagatcatgtttgagacc-3'; reverse primer: 5'-tttgctccaaccaactgc-3' (Fiorenza and Mangia, 1998); denaturation for 5 sec, and extension for 20 sec) were determined under similar conditions.

Different amounts of CYP2A5 (Su et al., 1998), CYP2F2 (generated with PCR according the sequence of Ritter et al. (1991)), and mouse β-actin (generated by PCR) cDNAs were used as standards for quantitation. Detection of fluorescence in each reaction was carried out at 3 ^{o}C below the melting temperature (Tm) of the corresponding PCR product. The specificity of the PCR products was confirmed by melting-curve analysis and by sequencing. Quantification and melting temperature analysis were performed using the LightCycler Data Analysis software.

Genotyping *Cyp2a5* in *Cyp2g1*$^{-/-}$ Mice. A 1.1-kb genomic fragment was amplified using forward (5'-cctgtattcaccatctacctgggac-3') and reverse primers (5'-cgcacagcaggtatcagcgtgc-3') complementary to exon 2 and intron 3 of *Cyp2a5*, respectively. The PCR products, which contain a polymorphic marker that distinguishes the *Cyp2a5* locus of 129/Sv strain (C) from that of the B6 strain (T), were analyzed by DNA sequencing to determine the strain from which the *Cyp2a5* gene in the knockout mice was derived.

Immunoblot Analysis and Quantitation. The relative levels of CYP and other biotransformation enzymes were determined by immunoblot, using the following antibodies: goat antibodies against rat CYP1A1/2, CYP2B1, CYP2C6, CYP3A2, and CPR (BD Gentest, Woburn, MA); rabbit anti-human CYP2E1 (Oxford Biomedical Research, Oxford, MI); rabbit anti-rat CYP2J4 (Zhang et al., 1998); rabbit anti-CYP2A5 (Gu et al., 1998); and rabbit anti-rat microsomal epoxide hydrolyase (a gift from Dr. Charles Kasper of the University of Wisconsin, Madison, WI). Microsomal preparation and immunoblot analysis were carried out essentially as described previously (Ding and Coon, 1990). Protein concentrations were determined by the bicinchoninic acid method (Pierce) with bovine serum albumin as the standard. The intensity of the detected bands was quantified with a densitometer (Personal Densitometer SI) and ImageQuant v5.0 software (Amersham Biosciences, Piscataway, NJ).

Determination of Catalytic Activity. Assays contained 50 mM potassium phosphate buffer, pH 7.4 (unless otherwise indicated); reactions were initiated by the addition of NADPH to a final concentration of 1 mM and carried out at 37^{o}C. Metabolism of testosterone and progesterone was assayed essentially as described earlier (Hua et al., 1997), with [1,2,6,7-^{3}H]testosterone (95 Ci/mmol) and [1,2,6,7-^{3}H]progesterone (104 Ci/mmol) (NEN Life Science, Boston, MA). Reaction mixtures contained 10 or 5 μM substrate, and 0.1 mg/ml microsomal protein. Reactions were carried out for 10 min (for testosterone) or 30 min (for progesterone). DCBN-protein adduct formation was assayed as described previously (Ding et al., 1996). Reaction mixtures contained OM microsomes (0.1 mg of protein/ml) and 2,6-[ring-^{14}C]DCBN (16.7 Ci/mol; Sigma, St Louis, MO) at a concentration of 3 or 30 μM. The reactions were carried out for 30 min. Coumarin 7-hydroxylase activities were assayed using a fluorometric method, with coumarin at 0.5 mM, or by radiometric HPLC, as described previously (Zhuo et al., 1999). For radiometric analysis of coumarin metabolites, the reaction mixtures contained 0.2 to 0.3 mg/ml microsomal protein and 20 or 72 μM [4-^{14}C]-coumarin (14.5 mCi/mmol, Sigma); reactions were carried out for 5 - 10 min. Metabolic activation of AP was assayed by a determination of the rates of formation of AP glutathione adduct (Gu et al., 1998). The reaction mixtures contained 50 mM potassium phosphate, pH 7.6, 0.05-0.5 mM AP, 10 mM reduced glutathione, 1 mM NADPH, and 0.3-1.0 mg/ml S9 fraction or microsomal proteins. For assays involving LNG, an NADPH-generating system (5 mM glucose 6-phosphate, 3 mM $MgCl_2$, 1mM $NADP^{+}$, and 1.5 U of glucose-6-phosphate dehydrogenase) was used in place of NADPH.

Animal Treatments. Animals were normally maintained at 22^{o}C with a 12-hr on, 12-hr off light cycle, and were allowed free access to water and a standard laboratory diet. For determination of circadian effects on CYP2A5 expression, animals were kept in the light-off

cycle for 4 days and were sacrificed at either 9 A.M. or 9 P.M., Eastern Standard Time, of the fifth day, using a protocol described by Lavery and coworkers (1999). The food-finding behavior test was performed according to Harding et al. (1978), using 2-month-old female mice. Animals were deprived of food overnight and were tested the next morning.

For determination of AP clearance and toxicity, animals were given a single i.p. injection (at 9-10 A.M. after overnight fasting) of AP (50 mg/ml in warm saline (Genter et al., 1998) or in 25% (w/v) PEG (Sigma) (Nishimura et al., 1999)), at a dose of 200, 400, or 600 mg/kg. Animals in the control groups received the corresponding vehicle only. Blood samples (15 μl each) were collected in heparin-coated capillaries by tail bleeding, at 15 min and 1, 2, 6, 8, and 12 hr after the injection, and were mixed with an equal volume of saline. The samples were spun at 800 x *g* for 5 min at 4^{o} C; the supernatant fraction was mixed with one-half volume of 1 M perchloric acid and spun again at 2000 x *g* for 5 min to remove precipitated proteins. Aliquots of the final supernatant were analyzed for AP concentration on an HPLC according to the method previously described (Gu et al., 1998).

At 24 hr after AP injection, surviving mice were sacrificed, and blood samples were collected by cardiac puncture. ALT levels were determined using a kit from Sigma Diagnostics (DG159-UV), with 10-50 μl of plasma. The liver tissue was collected and stored frozen at - 80^{o}C before analysis for the content of non-protein thiols, which was determined according to Tonge et al. (1998). Glutathione was used as a standard. The nasal tissues were fixed in Bouin's fixative or formaldehyde for histological examination, as described previously (Gu et al., 1997). The nasal cavity was sectioned at three levels (corresponding to levels 3, 5, and 6 in Young (1986)), embedded in paraffin, and stained with hematoxylin and eosin.

Dissection and Fractionation of LNG. The mouse head was trimmed to remove the eyes, skin, and lower jaw. The nose was cut, perpendicular to the hard palate and the nasal septum, at the second palatal ridge (Young et al., 1986). The LNG, which surrounds the maxillary turbinate, was identified on both sides of the cut under a dissection microscope and extracted with a fine-tipped surgical forceps. The wet weight of dissected LNG was about 5-6 mg per mouse. Tissues from at least three mice were pooled for the preparation of RNA, using the RNeasy Mini kit from Qiagen (Valencia, CA), and LNG of eight mice were pooled for the preparation of the postmitochondrial S9 fraction (Gu et al., 1997).

Results

Generation and General Characterization of *Cyp2g1*-null Mice. The structures of the wild-type *Cyp2g1* allele, the targeting construct, and the targeted *Cyp2g1*-null allele are shown in Figure 1, panels A-C. A *Cyp2g1* genomic clone isolated from the 129/Sv strain was used to construct the targeting vector. The strategy used for targeted disruption of the mouse *Cyp2g1* gene by homologous recombination in ES cells was to replace its exon 3, which presumably encodes parts of the substrate-binding site in enzymes of the *CYP2* subfamily, with a neomycin-resistance gene. Following electroporation, ES cell colonies that survived the double selection with G418 and ganciclovir were genotyped. Analyses of genomic DNA from ES cells with the probe H confirmed that six of 144 colonies examined (efficiency: 4.2%) were homologous recombinants; the 5.5-kb and 6.5-kb diagnostic fragments on Southern blots corresponding to the targeted allele and the wild-type allele, respectively. ES cells from a homologous recombinant cell line, designated 1D4, were injected into the blastocoel cavity of B6 embryos, from which 16 chimeric males were generated. When bred with wild-type B6 females, seven chimeras exhibited germline transmission. Homozygous mutant mice (*Cyp2g1*$^{-/-}$) were produced by crossbreeding the heterozygous littermates (*Cyp2g1*$^{+/-}$). Homozygotes, heterozygotes, and wild-type littermates were identified by the presence of the characteristic bands on Southern blots (Fig. 1, panel D).

The impact of the targeted mutation on *Cyp2g1* expression in the OM was examined by Northern blot analysis, with a full-length mouse CYP2G1 cDNA probe (Hua et al., 1997). As shown in Figure 1, panel E, two transcripts were found in the wild-type littermate (+/+), with the one of higher mobility being the major transcript. Abundance of the CYP2G1 transcripts was much lower in the heterozygote (+/-), whereas no signal was detected in the homozygous mutant

mouse (-/-). The absence of any positive signal in the *Cyp2g1*$^{-/-}$ mouse also indicated that a transcript from the targeted *Cyp2g1* allele was either not generated or not properly processed.

Mice homozygous for the disrupted allele were indistinguishable from their wild-type and heterozygous littermates in growth rate and reproductive ability. No deviation from Mendelian distribution was observed, suggesting that CYP2G1 is not important for embryonic development. No histological abnormalities were detected in the OM, brain, heart, lung, kidney, liver, small intestine, and testis of the *Cyp2g1*-null mice (data not shown). The *Cyp2g1*-null mice apparently had normal olfactory ability, as demonstrated in a food-finding behavior test; the *Cyp2g1*-null mice took 66 ± 23 s (n=8) to find a buried food pellet, which was not significantly different from the time taken by B6 (96 ± 63 s, n=8) or 129/Sv (67 ± 32 s, n=8) mice in the same experiment.

The expression of several other CYP enzymes, including CYP1A2, 2B, 2C, 2E1, 2J, and 3A, as well as CPR and microsomal epoxide hydrolase, was examined by immunoblot analysis of OM microsomes from *Cyp2g1*$^{-/-}$ mice and the parental wild-type strains as controls. As shown in Figure 2, expression levels were similar for each of these enzymes in OM microsomes of male and female B6, 129/Sv, and *Cyp2g1*$^{-/-}$ mice. Thus, disruption of the *Cyp2g1* gene did not cause compensatory increases in the expression of these enzymes in the OM.

Effects of *Cyp2g1* Mutation on *Cyp2a5* Expression. The *Cyp2g1*-null mice have a mixed genetic background (backcrossed twice: 75% B6 and 25% 129/Sv), and the expression and activity of CYP2A5 are known to be different in these two strains, as well as between genders (e.g. van Iersel et al., 1994). Sequence analysis of the CYP2A5 transcript from the *Cyp2g1*-null mice indicated that their *Cyp2a5* alleles were derived from the 129/Sv strain (data not shown). Thus, the 129/Sv strain was used as a wild-type control for determining the effects

of targeted *Cyp2g1* mutation on the expression and activity of CYP2A5. Expression of CYP2A5 mRNA in the liver is also known to be influenced by circadian rhythm (Lavery et al., 1999), although it is not known whether similar effects occur in extrahepatic tissues. Therefore, tissues were obtained at 9 A.M. or 9 P.M., when the hepatic CYP2A5 mRNA was expected to be at about the lowest and the highest level, respectively (Lavery et al., 1999). As shown in Table 1, the levels of CYP2A5 mRNA were lower in the *Cyp2g1*-null mice than in the 129/Sv mice, in the liver, kidney, and OM of either males or females, at either 9 A.M. or 9 P.M. However, the magnitude of the strain difference was much greater in liver and kidney than in the OM, where statistically significant differences were only seen at 9 P.M. Interestingly, the circadian effects on CYP2A5 mRNA level were dramatic in both liver and kidney, but were not significant in the OM. Furthermore, these effects were not altered by the disruption of the *Cyp2g1* gene, except in the kidneys of female mice.

Decreases (25%-75%) in CYP2A protein levels were also observed when microsomal preparations from liver and kidney of 129/Sv and *Cyp2g1*-null mice (male and female, at 9 A.M. or 9 P.M.) were analyzed with an antibody to CYP2A5 (data not shown). However, since the polyclonal antibody used probably reacts with mouse CYP2A4, CYP2A5, and CYP2A12, the level of CYP2A5 protein could not be determined using this approach. Similarly, the level of CYP2A5 protein could not be determined in the OM by immunoblot analysis, because the antibody also reacted with CYP2G1. Subsequently, the relative levels of CYP2A5 enzyme in the 129/Sv and *Cyp2g1*-null strains were estimated by a determination of microsomal activities in coumarin 7-hydroxylation, which is specific for CYP2A5 (Negishi et al., 1989). As shown in Table 2, the extent of decrease in coumarin 7-hydroxylase activities in liver and kidney of the *Cyp2g1*-null mice was more or less similar to the extent of decrease of the CYP2A5 mRNA

levels shown in Table 1. However, the differences in OM activity between the *Cyp2g1*-null and the 129/Sv strains were lower than the corresponding differences in the CYP2A5 mRNA levels, and were not seen in males at 9 A.M. Thus, there is a definitive and large decrease of CYP2A5 expression and activity in the liver and kidney of the *Cyp2g1*-null mice, but a much smaller decrease in the OM. In addition, the activities in liver and kidney were only slightly higher at 9 P.M. than at 9 A.M., in contrast to the very large differences seen in mRNA levels; in the OM, the activity was apparently lower at 9 P.M. than at 9 A.M.

In light of the unexpected, large decreases in CYP2A5 level in the livers of the *Cyp2g1*-null mice, the hepatic expression of several other CYPs was also examined. Immunoblot analysis with liver microsomes from adult male and female mice (sacrificed at about 9 A.M.; microsomes prepared from combined tissues of three animals per group) indicated that the levels of CYP2B, CYP2C, CYP2E1, CYP3A, as well as CPR were similar in microsomes from the *Cyp2g1*-null mice and those from the B6 and 129/Sv strains (data not shown). In other experiments not presented, the levels of CYP2F2 mRNA were determined by RNA-PCR in tissues obtained at 9 A.M. Although *Cyp2f2* was not detected in the *Cyp2g1*-containing BAC clone (data not shown), it is expected to be located in the *Cyp2* gene cluster on chromosome 7, and therefore may also be impacted by changes in the *Cyp2g1* gene. However, the results showed that the level of CYP2F2 mRNA was not different among the three strains, although the levels were about three times as high in males than in females in all strains.

Role of CYP2G1 in the Metabolism of Steroid Hormones and Nasal Toxicants in OM Microsomes. The results in Table 2 indicated that the levels of OM CYP2A5 activity are not significantly different between the *Cyp2g1*$^{-/-}$and 129/Sv mice, at least in males. This was confirmed by additional studies using lower concentrations of coumarin, as shown in Table 3. In

these studies, no significant difference in coumarin 7-hydroxylase activities was seen between the two strains, with coumarin at either 20 μM or 72 μM. Therefore, it was possible to determine the specific roles of CYP2G1 in OM microsomal metabolism for compounds known to be substrates of both CYP2A5 and CYP2G1, including testosterone, progesterone, DCBN, and coumarin (Gu et al., 1998; 1999; Hua et al., 1997; Zhuo et al., 1999). The substrate concentrations used were chosen to minimize the potential contribution of other CYPs with higher K_m values than those of CYP2G1. In addition, although 129/Sv mice are the proper control for the *Cyp2g1*-null mice (because of the genotype of the *Cyp2a5* locus), the activities of B6 mice were also examined to detect possible confounding by other strain-related differences in CYP activity.

As shown in Table 3, the rates of formation of 15α-hydroxy testosterone, the major metabolite generated in OM microsomes, and the combined rates of formation of the two nasal microsomal progesterone metabolites, which remain to be identified (Hua et al., 1997), were about 60% lower in the *Cyp2g1*-null mice than in the 129/Sv mice. The extent of decrease is even greater when compared with rates in the B6 mice. Thus, CYP2G1 clearly plays a major role in microsomal metabolism of these sex steroids in the OM. CYP2G1 also appears to play the dominant role in OM microsomal activation of coumarin: the rates of formation of *o*-HPA were almost 80% lower in the *Cyp2g1*-null mice than in the 129/Sv strain. Again, the extent of activity decrease is greater when compared with the B6 strain. On the other hand, CYP2G1 may not play a major role in OM microsomal metabolism of DCBN; a statistically significant difference was not found between *Cyp2g1*-null and 129/Sv mice in the rates of formation of DCBN-protein adduct.

Impact of *Cyp2g1* Disruption on AP Metabolism and Toxicity *in vivo*. The reduction in CYP2A5 expression in the liver and kidney of the *Cyp2g1*-null mice suggested that this mouse model might have a decreased systemic clearance of those drugs that are CYP2A5 substrates. The *in vivo* clearance and toxicity of a known CYP2A5 substrate, AP, was therefore examined. As shown in Table 4, there was no decrease in AP clearance following a single i.p. injection at 400 or 600 mg/kg in the *Cyp2g1*-null mice. There was also no significant difference in the extent of hepatotoxicity among the three strains, as indicated by the survival rate and by levels of plasma ALT and hepatic total non-protein thiols at 24 hr after treatment (Table 5). Thus, hepatic CYP2A5 does not seem to play a significant role in the clearance or hepatotoxicity of AP *in vivo*, which was confirmed by *in vitro* studies (not shown) indicating that rates of liver microsomal metabolism of AP (at a substrate concentration of 50 μM) to glutathione adduct were not significantly different between *Cyp2g1*-null mice and B6 or 129/Sv mice.

AP treatment also caused toxicity in the nasal cavity, as has been reported previously (Genter et al., 1998). The most striking lesions were in the LNG (Fig. 3), and consisted of mild to moderate, multifocal to locally extensive necrosis, characterized by loss of glandular epithelial cell granules, as well as nuclear pyknosis or karyorrhexis of glandular or ductal epithelium. Interestingly, the *Cyp2g1*-null mice were resistant to AP toxicity in the LNG at a dose of 400 mg/kg (Table 5 and Fig. 3). These mice also seemed to be less sensitive to AP toxicity than were the wild-type strains at 600 mg/kg, although the numbers of surviving mice in each group were not sufficient to draw definitive conclusions (Table 5). The site-specific, protective effects of *Cyp2g1* gene disruption on the extent of AP cytotoxicity in the LNG were also observed when AP was administrated in saline, which yielded lower plasma AP levels than when AP was injected in PEG (data not shown)

Other lesions in the nasal cavity included degeneration and necrosis of respiratory epithelium; sloughing of epithelial cells of nasolacrimal duct into lumen; degeneration or detachment of olfactory epithelium; necrosis of submucosal serous glands, including Bowman's glands; and lympholysis of lymphocytes in the mucosa-associated lymphoid tissue. However, there was no clear difference in the extent of AP toxicity in these structures among the three strains (not shown). No lesion was found in vehicle-treated B6, 129/Sv, or *Cyp2g1*-null mice. The apparent lack of effects of *Cyp2g1* gene disruption on the extent of AP cytotoxicity in the OM is consistent with results from *in vitro* studies with OM postmitochondrial S9 fractions, which indicated only a small (about 20-30%) decrease at a substrate concentration of 50 or 100 μM (data not shown), and no decrease at 0.5 mM (Table 6), in the rates of AP metabolism to glutathione adducts in *Cyp2g1*-null mice, relative to B6 or 129/Sv mice.

The site-specific, protective effects of *Cyp2g1* gene disruption on the extent of AP cytotoxicity in the LNG prompted further analysis of CYP expression in this organ. RNA-PCR analysis of dissected LNG detected CYP2A5, but not CYP1A2 or CYP2G1 (Fig. 4, panel A). The identity of the LNG CYP2A5 PCR product was confirmed by sequencing. The level of CYP2A protein in the LNG S9 fraction was much lower in the *Cyp2g1*-null mice than in the wild-type control mice (Fig. 4, panel B); densitometric analysis indicated that the levels in the *Cyp2g1*-null mice were less than 10% of the levels detected in the B6 or 129/Sv mice. The reduction in LNG CYP2A protein level was confirmed by decreases in coumarin 7-hydroxylase activity; however, the rates of *in vitro* metabolic activation of AP by LNG S9 fractions were very low, compared with those of the OM S9 fractions from the same animals, and were not decreased in the *Cyp2g1*-null mice (Table 6).

Discussion

The *Cyp2g1*$^{-/-}$ mice generated in this study are viable and fertile, and they develop normally and do not show signs of severe olfactory deficits. There appear to be no marked compensatory changes in the expression of the other P450 enzymes in the OM of *Cyp2g1*-null mice. Thus, CYP2G1 appears to be nonessential in mice for development, reproduction, and olfactory chemoreception. On the other hand, despite the potential for complications by strain- and sex-dependent differences in microsomal metabolic activities, we were able to show that mouse CYP2G1 is the major P450 involved in microsomal metabolism of testosterone and progesterone, and in the metabolic activation of coumarin in the OM. Thus, this animal model will be valuable for assessing the contribution of CYP2G1 to nasal metabolism of other steroid hormones, odorants, drugs, and toxicants. Furthermore, initial studies of the impact of *Cyp2g1* knockout on AP toxicity led to an intriguing discovery that the LNG, a previously unidentified target organ for AP toxicity, became resistant to AP in the *Cyp2g1*-null mice at AP doses that caused toxicity to the OM and liver, despite the fact that CYP2G1 is not normally expressed in the LNG. We propose that OM CYP2G1 (through a paracrine pathway) or LNG CYP2A5 may indirectly influence resistance of the LNG to chemical toxicity, possibly by regulating gene expression in the LNG through steroid hormones or other endogenous CYP substrates and their metabolites.

A significant reduction in the expression of the *Cyp2a5* gene was found in the liver, the LNG, and, to a lesser extent, the kidney, of adult *Cyp2g1*-null mice. This unexpected neighboring effect of *Cyp2g1* knockout on *Cyp2a5* expression in liver makes the *Cyp2g1*-null mouse model a useful tool for assessing the role of hepatic CYP2A5 in systemic metabolism of endogenous as well as foreign chemicals, but it could also complicate attempts to apply this

model to studies on the role of CYP2G1 in local metabolism and toxicity of systemically administered chemicals that are also CYP2A5 substrates. In this regard, because the decrease in CYP2A5 expression did not reduce systemic clearance or the extent of AP hepatotoxicity, we were able to use the *Cyp2g1*-null mice to probe the role of CYP2G1 in AP nasal toxicity. On the other hand, although OM coumarin toxicity is likely mediated by CYP2G1, this hypothesis was not tested in the current study, because CYP2A5 is the major coumarin hydroxylase in the liver (Negishi et al., 1989), and because the *Cyp2a5* gene has a strain-related genetic polymorphism that significantly affects coumarin hydroxylase activity (Lindberg et al., 1992). It is likely that the impact of an altered hepatic CYP2A5 expression on OM toxicity will be less worrisome for compounds delivered through the nose. The lack of effect of CYP2A5 down-regulation on systemic clearance and hepatic toxicity of AP is consistent with previous findings indicating that CYP2E1 and CYP1A2 are major contributors to AP metabolism and toxicity in the liver (Genter et al., 1998; Tonge et al., 1998; Zaher et al., 1998).

Several CYPs known to be expressed in the OM are active in the metabolic activation of AP (Gu et al., 1998), which may explain why OM microsomes from *Cyp2g1*-null mice had only slightly lower turnover numbers for AP than those in wild-type mice (at low substrate concentrations), and why *Cyp2g1*-null mice were not protected against AP toxicity to the OM. However, the resistance of the LNG to AP toxicity in the *Cyp2g1*-null mice is intriguing. On one hand, the down-regulation of CYP2A5, which is active in the metabolic activation of AP (Gu et al., 1998), appears to provide a logical explanation; the absence of CYP2G1 and CYP1A2 would make the contribution of CYP2A5 to local AP metabolism much more significant in the LNG than in the OM. However, *in vitro* analysis indicated that activity of AP metabolic activation was very low in the LNG, and was apparently not reduced in the *Cyp2g1*-null mice. Thus, the

protective effect seen in the LNG of the *Cyp2g1*-null mice may not be related to a decreased local metabolic activation of AP. Instead, the loss of CYP2G1 in the OM or the down-regulation of CYP2A5 in the LNG (or both) may have resulted in altered metabolism and homeostasis of an endogenous substrate(s), such as a steroid hormone, that is important for the defense of the LNG against AP toxicity. Further studies to confirm this hypothesis are warranted, and the results may have general implications on the endogenous functions of microsomal "drug-metabolizing" CYP enzymes in various extrahepatic tissues.

The mechanism of chemically induced LNG toxicity is not clear. Although *in vitro* activity of LNG S9 fractions seemed to be very low, the LNG has been found to have significant bioactivation activities *in vivo*; many compounds have been shown to be bioactivated in the LNG following systemic administration (e.g., Castonguay et al., 1983). Few studies have examined P450 expression in the LNG (Adams et al., 1991; Chen et al., 1992). In this study, we have obtained definitive evidence for the expression of CYP2A5, and for the lack of expression of CYP1A2 and CYP2G1, in mouse LNG. Nevertheless, the role of LNG P450s in target tissue toxicity remains to be determined. Additionally, the potential impact of chemically induced LNG degeneration on the production of odorant-binding proteins or on the local immune function will be interesting topics to pursue.

Both *Cyp2a5* and *Cyp2g1* are predominantly expressed in the OM (for a review, see Ding and Dahl, 2003). The genes are adjacent to one another on chromosome 7, with *Cyp2g1* immediately (less than 20 kb) upstream of *Cyp2a5* (Wang et al., 2003). The mechanism of *Cyp2a5* suppression in the *Cyp2g1*-null mice has not been identified. However, neighboring effects of gene targeting have been documented previously for other genes (for a review, see Olson et al., 1996). In the present case, the *neo* gene, which replaces exon 3 of *Cyp2g1*, was

retained in the targeted allele; it was oriented in the same transcriptional direction as the *Cyp2g1* gene and the downstream *Cyp2a5* gene. It is likely that active transcription of the *neo* gene in tissues that normally have an inactive *Cyp2g1* allele (such as the liver and the LNG) disturbed the chromosomal structure at the *Cyp2a5* promoter, thereby leading to suppression of *Cyp2a5* transcription. On the other hand, since the *Cyp2g1* locus was normally active in the OM, the effects of *neo* insertion on *Cyp2a5* expression would be less pronounced. Further studies on this tissue-selective neighboring effect, such as studies on the nature and sites of chromosomal alternations in the liver and OM, may shed new light on the mechanisms of tissue-selective expression of the *CYP2A* genes.

The neighboring effect of *Cyp2g1* disruption was most likely limited to the *Cyp2a5* gene. This is supported by the observation that hepatic expression of *Cyp2f2*, which is about 250 kb downstream of *Cyp2a5* (Wang et al., 2003), was not affected. Although it is not clear at present which of the CYP2B proteins were detected in liver microsomes by the polyclonal anti-CYP2B antibody, the lack of alteration in the overall intensity of the detected CYP2B bands suggests that the expression of the *Cyp2b* genes, which are about 40 to 950 kb upstream of *Cyp2g1* (Wang et al., 2003), was not affected either. The first identified gene downstream of *Cyp2a5* appears to be a *Cyp2a* pseudogene (*Cyp2a23p*), about 65 kb away (Wang et al., 2003).

The dramatic circadian variation in the level of hepatic and renal CYP2A5 mRNA was not altered by the disruption of the *Cyp2g1* gene (except in case of female kidney), despite overall decreases in CYP2A5 mRNA levels in these tissues. Previous studies by Lavery et al. (1999) had indicated that, in the liver, this circadian effect was partly controlled by the transcription factor DBP (albumin D-site-binding protein). Interestingly, we observed that the

circadian variation in CYP2A5 mRNA level was essentially undetectable in the OM, a fact which implicates tissue differences in the role of this transcription factor at the *Cyp2a5* promoter.

The complex and poorly characterized strain variations in the expression and activity of various microsomal *Cyp* genes and enzymes remain a major challenge for studies using *Cyp*-null mouse models. In our *Cyp2g1*-null model, which is on a mixed B6 and 129/Sv background, the close linkage between *Cyp2g1* and *Cyp2a5* dictates that the *Cyp2a5* gene is derived from the 129/Sv strain, from which the CJ7 ES cells used for gene targeting were derived. In contrast, the *Cyp2a5* gene in the wild-type littermates is derived from the B6 strain. Other nearby *Cyp2* genes will also likely co-segregate with the targeted *Cyp2g1* allele, and therefore will likely be derived from the 129/Sv strain. Both *Cyp2a5* (Lindberg et al., 1992) and *Cyp2g1* (Zhuo et al., 2001) have coding region polymorphisms that may have contributed to the strain differences in microsomal activities seen in this study. Therefore, it was necessary to use both parental strains as controls in most of the experiments, which may have resulted in an underestimation of the contributions of CYP2G1 in some cases.

Acknowledgments

We are grateful to Diane Decker for assistance with histological analysis of mouse tissues and Mingfei Luo for contributing to the characterization of the CYP2G1 BAC clone. The authors gratefully acknowledge the use of the Transgenic and Knockout Mouse Core, the Molecular Genetics Core, and the Biochemistry Core of the Wadsworth Center. We thank Drs. Laurence Kaminsky and Adriana Verschoor for reading the manuscript.

References

Adams DR, Deyoung DW, and Griffith R (1981) The lateral nasal gland of dog: its structure and secretory content. *J Anat* **132**:29-37.

Adams DR, Jones AM, Plopper CG, Serabjit-Singh CJ, and Philpot RM (1991) Distribution of cytochrome P-450 monoxygenase enzymes in the nasal mucosa of hamster and rat. *Am J Anat* **190**:291-298.

Belinsky SA, Walker VE, Maronpot RR, Swenberg JA, and Anderson MW (1987) Molecular dosimetry of DNA adduct formation and cell toxicity in rat nasal mucosa following exposure to the tobacco specific nitrosamine 4-(N-methyl-N-nitrosamino)-1-(3-pyridyl)-1-butanone and their relationship to induction of neoplasia. *Cancer Res* **47**:6058-6065.

Castonguay A, Tjalve H, and Hecht SS (1983) Tissue distribution of the tobacco-specific carcinogen 4-(methylnitrosamino)-1-(3-pyridyl)-1-butanone and its metabolites in F344 rats. *Cancer Res* **43**:630-638.

Chen Y, Getchell ML, Ding X, and Getchell TV (1992) Immunolocalization of two cytochrome P450 isozymes in rat nasal chemosensory tissue. *Neuroreport* **3**:749-752.

Ding X, Spink DC, Bhama JK, Sheng JJ, Vaz AD, and Coon MJ (1996) Metabolic activation of 2,6-dichlorobenzonitrile, an olfactory-specific toxicant, by rat, rabbit, and human cytochromes P450. *Mol Pharmacol* **49**:1113-1121.

Ding X and Coon MJ (1990) Immunochemical characterization of multiple forms of cytochrome P-450 in rabbit nasal microsomes and evidence for tissue-specific expression of P-450s NMa and NMb. *Mol Pharmacol* **37**:489-496.

Ding X and Dahl AR (2003) Olfactory mucosa: composition, enzymatic localization, and metabolism, in *Handbook of Olfaction and Gustation*, 2nd Ed (Doty RL ed) pp 51-73,

Marcel Dekker, New York

Fiorenza MT and Mangia F (1998) Quantitative RT-PCR amplification of RNA in single mouse oocytes and preimplantation embryos. *Biotechniques* **24**:618-623.

Genter MB, Liang HC, Gu J, Ding X, Negishi M, McKinnon RA, and Nebert DW (1998) Role of CYP2A5 and 2G1 in acetaminophen metabolism and toxicity in the olfactory mucosa of the Cyp1a2(-/-) mouse. *Biochem Pharmacol* **55**:1819-1826.

Getchell ML and Mellert TK (1991) Olfactory mucus secretion, in *Smell and Taste in Health and Disease* (Getchell TV, Doty RL, Bartoshuk LM, and Snow JB, Jr eds) pp 83-95, Raven Press, New York

Gu J, Dudley C, Su T, Spink DC, Zhang QY, Moss RL, and Ding X (1999) Cytochrome P450 and steroid hydroxylase activity in mouse olfactory and vomeronasal mucosa. *Biochem Biophys Res Commun* **266**:262-267.

Gu J, Walker VE, Lipinskas TW, Walker DM, and Ding X (1997) Intraperitoneal administration of coumarin causes tissue-selective depletion of cytochromes P450 and cytotoxicity in the olfactory mucosa. *Toxicol Appl Pharmacol* **146**:134-143.

Gu J, Zhang QY, Genter MB, Lipinskas TW, Negishi M, Nebert DW, and Ding X (1998) Purification and characterization of heterologously expressed mouse CYP2A5 and CYP2G1: role in metabolic activation of acetaminophen and 2,6-dichlorobenzonitrile in mouse olfactory mucosal microsomes. *J Pharmacol Exp Ther* **285** :1287-1295.

Harding JW, Getchell TV, and Margolis FL (1978) Denervation of the primary olfactory pathway in mice. V. Long-term effect of intranasal ZnSO4 irrigation on behavior, biochemistry and morphology. *Brain Res* **140**:271-285.

Hogan B, Bedelington R, Costantini F, and Lacy E (1994) *Manipulating the Mouse Embryo: A*

Laboratory Manual, 2nd Ed, Cold Spring Harbor Laboratory, Cold Spring Harbor, NY

Hua Z, Zhang QY, Su T, Lipinskas TW, and Ding X (1997) cDNA cloning, heterologous expression, and characterization of mouse CYP2G1, an olfactory-specific steroid hydroxylase. *Arch Biochem Biophys* **340**:208-214.

Lavery DJ, Lopez-Molina L, Margueron R, Fleury-Olela F, Conquet F, Schibler U, and Bonfils C (1999) Circadian expression of the steroid 15 alpha-hydroxylase (Cyp2a4) and coumarin 7-hydroxylase (Cyp2a5) genes in mouse liver is regulated by the PAR leucine zipper transcription factor DBP. *Mol Cell Biol* **19**:6488-6499.

Lindberg RL, Juvonen R, and Negishi M (1992) Molecular characterization of the murine Coh locus: an amino acid difference at position 117 confers high and low coumarin 7-hydroxylase activity in P450coh. *Pharmacogenetics* **2**:32-37.

Mansour SL, Thomas KR, and Capecchi MR (1988) Disruption of the proto-oncogene int-2 in mouse embryo-derived stem cells: a general strategy for targeting mutations to non-selectable genes. *Nature* **336**:348-352.

Moe H and Bojsen-Moller F (1971) The fine structure of the lateral nasal gland (Steno's gland) of the rat. *J Ultrastruct Res* **36**:127-148.

Morgan DL, Mahler JF, Wilson RE, Moorman MP, Price HC, Jr., and O'connor RW (1997) Toxicity of divinylbenzene-55 for B6C3F1 mice in a two-week inhalation study. *Fund Appl Toxicol* **39**:89-100.

Negishi M, Lindberg R, Burkhart B, Ichikawa T, Honkakoski P, and Lang M (1989) Mouse steroid 15 alpha-hydroxylase gene family: identification of type II P-450(15)alpha as coumarin 7-hydroxylase. *Biochemistry* **28**:4169-4172.

Nishimura Y, Kurata N, Iwase M, Li H, and Yasuhara H (1999) The effects of organic solvents

on trimethadione n-demethylation in rats. *Res Commun Mol Pathol Pharmacol* **104**:229-239.

Olson EN, Arnold HH, Rigby PW, and Wold BJ (1996) Know your neighbors: three phenotypes in null mutants of the myogenic bHLH gene MRF4. *Cell* **85**:1-4.

Ritter JK, Owens IS, Negishi M, Nagata K, Sheen YY, Gillette JR, and Sasame HA (1991) Mouse pulmonary cytochrome P-450 naphthalene hydroxylase: cDNA cloning, sequence, and expression in Saccharomyces cerevisiae. *Biochemistry* **30**:11430-11437.

Snyder SH, Sklar PB, and Pevsner J (1988) Molecular mechanisms of olfaction. *J Biol Chem* **263**:13971-13974.

Soriano P, Montgomery C, Geske R, and Bradley A (1991) Targeted disruption of the c-src proto-oncogene leads to osteopetrosis in mice. *Cell* **64**:693-702.

Stewart CL, Kaspar P, Brunet LJ, Bhatt H, Gadi I, Kontgen F, and Abbondanzo SJ (1992) Blastocyst implantation depends on maternal expression of leukaemia inhibitory factor. *Nature* **359**:76-79.

Su T, He W, Gu J, Lipinskas TW, and Ding X (1998) Differential xenobiotic induction of CYP2A5 in mouse liver, kidney, lung, and olfactory mucosa. *Drug Metab Dispos* **26**:822-824.

Swiatek PJ and Gridley T (1993) Perinatal lethality and defects in hindbrain development in mice homozygous for a targeted mutation of the zinc finger gene Krox20. *Genes Dev* **7**:2071-2084.

Tonge RP, Kelly EJ, Bruschi SA, Kalhorn T, Eaton DL, Nebert DW, and Nelson SD (1998) Role of CYP1A2 in the hepatotoxicity of acetaminophen: Investigations using Cyp1a2 null mice. *Toxicol Appl Pharmacol* **153**:102-108.

van Iersel ML, Walters DG, Price RJ, Lovell DP, and Lake BG (1994) Sex and strain differences in mouse hepatic microsomal coumarin 7-hydroxylase activity. *Food Chem Toxicol* **32**:387-390.

Wang H, Donley KM, Keeney DS, Hoffman SMG (2003) Organization and evolution of the *Cyp2* gene cluster on mouse chromosome 7, and comparison with the syntenic human cluster. *Environ Health Perspect* in press.

Young JT (1986) Light microscopic examination of the rat nasal passages: preparation and morphologic features, in *Toxicology of the Nasal Passages* (Barrow CS ed) pp 7-36, Hemisphere Publishing Corporation, NY

Zaher H, Buters JTM, Ward JM, Bruno MK, Lucas AM, Stern ST, Cohen SD, and Gonzalez FJ (1998) Protection against acetaminophen toxicity in CYP1A2 and CYP2E1 double-null mice. *Toxicol Appl Pharmacol* **152**:193-199.

Zhang QY, Raner G, Ding X, Dunbar D, Coon MJ, and Kaminsky LS (1998) Characterization of the cytochrome P450 *CYP2J4* - expression in rat small intestine and role in retinoic acid biotransformation from retinal. *Arch Biochem Biophys* **353**:257-264.

Zhang QY, Dunbar D, and Kaminsky LS (2003) Characterization of mouse small intestinal cytochrome P450 expression. *Drug Metab Dispos* in press.

Zhuo X, Gu J, Zhang QY, Spink DC, Kaminsky LS, and Ding X (1999) Biotransformation of coumarin by rodent and human cytochromes P-450: metabolic basis of tissue-selective toxicity in olfactory mucosa of rats and mice. *J Pharmacol Exp Ther* **288**:463-471.

Zhuo XL, Schwob JE, Swiatek PJ, and Ding X (2001) Mouse Cyp2g1 gene: Promoter structure and tissue-specific expression of a *Cyp2g1-LacZ* fusion gene in transgenic mice. *Arch Biochem Biophys* **391**:127-136.

Footnotes

This work was supported in part by Public Health Service grant ES07462 from the National Institute of Environmental Health Sciences, National Institutes of Health.

[†]Current address: Cancer Pharmacology, 1246 BRB II/III, University of Pennsylvania, 421 Curie Boulevard, Philadelphia, PA19104-6160

[‡]Current address: Van Andel Research Institute, 333 Bostwick NE, Grand Rapids, MI 49503.

FIGURE LEGENDS

Fig. 1. Targeted disruption of the mouse *Cyp2g1* gene. A-C, structures of the *Cyp2g1* wild-type allele, targeting vector, and targeted allele, respectively. Probe H, shown as a hatched box, was used to distinguish the wild-type and targeted alleles in Southern blot analysis. PCR primers E2U, NeoL, and E3L are indicated by short arrows. Restriction sites displayed include *Bam*H I (B), *Pst* I (P), *Hind* III (H), and *Sal* I (S). Exons are shown as solid boxes, and introns and flanking regions as solid lines. The *neo* and *tk* genes and their orientations are indicated. D, detection of the targeted *Cyp2g1* allele by Southern blot analysis of mouse tail genomic DNA. The 5.6-kb and 6.5-kb bands (detected with Probe H) represent the targeted (-) and wild-type (+) alleles, respectively. E, lack of CYP2G1 expression in the OM of *Cyp2g1*-null mice. Total RNA (15 μg each) from the OM of a 18-day-old wild-type (+/+), heterozygous (+/-), or homozygous (-/-) mutant male littermate was analyzed on a Northern blot with a [^{32}P]-labeled full-length mouse CYP2G1 cDNA probe. Positions of the 18S and 28S ribosomal RNAs are indicated by arrows.

Fig. 2. Absence of any compensatory increase in biotransformation enzymes in the OM following targeted disruption of the *Cyp2g1* gene. OM microsomes (2 μg) were analyzed in duplicate on Western blots. The antibodies used for the detection of CYP and epoxide hydrolase (EH) are described in Materials and Methods. Microsomes were prepared from pooled OM from three to five male or female mice (6 - 8 weeks old). Densitometric analysis indicated that, in each panel, the maximal difference in band intensity between samples from different animal groups was less than 30%. The top band detected by anti-CYP3A in some samples represents a non-specific signal.

Fig. 3. Histological analysis of AP toxicity in the LNG. Male, 3-month-old wild-type and *Cyp2g1*-null mice were treated with AP as described in the legend to Table 5. All sections were at the level of the second palatal ridge (level 5 in Young et al., 1986). A, cross section of the nasal cavity (of a 129/Sv mouse) at low magnification. The rectangular box marks the area shown in B and C at 100X magnification. ET, ethmoturbinate; MS, maxillary sinus; LNG, lateral nasal gland; SP, nasal septum. B, the LNG in this AP-treated *Cyp2g1*-null mouse had normal, palely staining cuboidal duct cells (DC) with open face nuclei and plump secretary cells (SC) with bright eosinophilic cytoplasmic granules. A 400X view is shown in D. C, the LNG in this AP-treated 129/Sv mouse had dark, shrunken duct cells (✻), congested vessel (CV), and pale, ragged secretary cells (PSC). At 400X magnification (E), additional signs of cytotoxicity can been seen, including apoptotic glandular epithelial cells (arrowheads), karyorrhexis (arrows), cytoplasmic fragmentation with loss of secretary granules (circles), and nuclear condensation in the shrunken ductal epithelial cells (✻). Scale bar represents 400 μm in A, 30 μm in B and C, and 10 μm in D and E.

Fig. 4. CYP Expression in the LNG. A, detection of CYP1A2, CYP2A5, and CYP2G1 mRNA by RNA-PCR. RNA from OM (as a positive control) and LNG of B6 mice was analyzed as described in Materials and Methods. The positions of selected fragments of a 100-bp DNA marker are indicated. B, immunoblot analysis of CYP2A expression in the LNG of *Cyp2g1*-null (KO) and wild-type C57BL/6 and 129/Sv mice. S9 fractions were prepared from pooled LNG of eight 2-month-old female mice in each group. Equal amounts of protein (10 μg) were analyzed in each lane with an antibody to CYP2A5.

JPET Fast Forward. Published on November 10, 2003 as DOI: 10.1124/jpet.103.060301
This article has not been copyedited and formatted. The final version may differ from this version.

TABLE 1

Effects of targeted *Cyp2g1* mutation on CYP2A5 mRNA level

Male and female mice at 12-16 week of age were kept in the dark for 4 days and sacrificed at about 9 A.M. or 9 P.M. on the fifth day. Total RNA was isolated from tissues of individual mice, and used for quantitative RNA-PCR analysis using a LightCycler. The values presented are means ± S.D. (n=3). The relative CYP2A5 mRNA levels in each pair of 129/Sv vs. *Cyp2g1*-null groups are significantly different ($p<0.05$), unless otherwise indicated. The difference between corresponding groups at 9 A.M. and 9 P.M. is also significant ($p<0.05$), unless otherwise indicated.

Tissue		Relative CYP2A5 mRNA Level (molar ratio of CYP2A5 to β-actin mRNA)					
		9 A.M.			9 P.M.		
		129/Sv	*Cyp2g1*-null	Ratio (%)[a]	129/Sv	*Cyp2g1*-null	Ratio (%)[a]
Male	OM	400±130	260±92[b]	65	680±180[c]	270±18[c]	39
	Liver	0.87±0.20	0.08±0.05	9	69±12	9.2±4.8	13
	Kidney	1.26±0.48	0.41±0.08	33	10±2	2.4±0.6	24
Female	OM	540±54	330±150[b]	61	420±100[c]	200±55[c]	47
	Liver	8.5±2.8	0.67±0.35	8	320±89	40±19	12
	Kidney	0.40±0.16	0.16±0.09[b]	40	4.8±2.6	0.27±0.13[c]	6

[a] *Cyp2g1*-null over 129/Sv.

[b] Not significantly different when compared to 129/Sv mice; $p>0.05$ (Student's t-test).

[c] Not significantly different when compared to corresponding groups at 9 A.M. ($p>0.05$).

JPET Fast Forward. Published on November 10, 2003 as DOI: 10.1124/jpet.103.060301
This article has not been copyedited and formatted. The final version may differ from this version.

TABLE 2

Effects of targeted *Cyp2g1* mutation on microsomal coumarin 7-hydroxylase activity

Male and female mice at 12-16 wk of age were kept in the dark for 4 days and sacrificed at about 9 A.M. or 9 P.M. on the fifth day. For microsomal preparation, liver and kidney from individual mice were used, whereas OM was pooled from three mice. Reaction mixtures contained 0.5 mM coumarin and 0.2, 0.4, or 0.8 mg/ml microsomal protein (for OM, liver and kidney, respectively). The reactions were carried out for 10 to 15 min, during which product formation was linear with time. Formation of 7-hydroxycoumarin was determined fluorometrically. Values presented are means ± SD (n=3) of duplicate determinations for liver and kidney, or means of triplicate determinations for pooled OM (with variations less than 10% of the mean). For liver and kidney, the turnover numbers in each pair of 129/Sv vs. *Cyp2g1*-null groups are significantly different ($p<0.05$), unless otherwise indicated. However, the difference between corresponding groups at 9 A.M. and 9 P.M. is *not* significant ($p>0.05$), unless otherwise indicated.

Tissue		Rate of Formation of 7-hydroxycoumarin (pmol/min/mg microsomal protein)					
		9 A.M.			9 P.M.		
		129/Sv	*Cyp2g1*-null	Ratio (%)[a]	129/Sv	*Cyp2g1*-null	Ratio (%)[a]
Male	OM	6000	6200	103	5700	4200	74
	Liver	200±50	46±13	23	400±76[c]	76±36	19
	Kidney	43±19	18±4[b]	42	65±7	19±3	29
Female	OM	9700	6800	70	5300	3400	64
	Liver	1000±190	160±89	16	1400±580	210±83	15
	Kidney	24±8	7±2	29	66±29	14±5	21

[a] *Cyp2g1*-null over 129/Sv.

[b] Not significantly different from 129/Sv mice; $p>0.05$.

[c] Significantly higher than the corresponding group at 9 A.M. ($p=0.019$).

JPET Fast Forward. Published on November 10, 2003 as DOI: 10.1124/jpet.103.060301
This article has not been copyedited and formatted. The final version may differ from this version.

TABLE 3

Effects of *Cyp2g1* knockout on OM microsomal activity toward testosterone, progesterone, DCBN, and coumarin

Male B6, 129/Sv and *Cyp2g1*-null mice were maintained with a 12-hr on, 12-hr off light cycle and sacrificed between 9 A.M. and 12 P.M. Each microsomal sample was prepared from pooled OM of three to five mice (3-4 month old for coumarin assay, and 6-8 weeks old for the other substrates). Values reported are mean ± S.D. (n = 3) of initial linear rate. Contents of reaction mixtures and assay procedures are described in Materials and Methods. The rates of formation of 15α-hydroxytestosterone from testosterone, total metabolites (P1 and P2) from progesterone (Gu et al., 1999), DCBN-protein adducts from DCBN, *o*-HPA and 7-hydroxycoumarin from coumarin were determined. The turnover numbers in each pair of 129/Sv and B6 groups or between the 129/Sv and *Cyp2g1*-null groups are significantly different ($p<0.05$), unless otherwise indicated.

Substrate	Product	Rates of Product Formation (pmol/min/mg microsomal protein)			Ratio *Cyp2g1*-null :129/Sv (%)
		B6	129/Sv	*Cyp2g1*-null	
Coumarin (20 μM)	7-Hydroxycoumarin	1000±200	4600±200	4000±1400[a]	87
Coumarin (72 μM)	7-Hydroxycoumarin	1500±500	4600±1100	3100±100[a]	67
Coumarin (20 μM)	*o*-HPA	3100±500	1400±300	300±100	21
Coumarin (72 μM)	*o*-HPA	4200±800	1100±100	300±100	27
Testosterone (5 μM)	15α-Hydroxytestosterone	940±120	690±20	260±20	38
Testosterone (10 μM)	15α-Hydroxytestosterone	1100±150	740±130	300±40	40
Progesterone (5 μM)	P1 + P2	510±40	290±40	110±10	38
Progesterone (10 μM)	P1 + P2	400±100	340±20[b]	150±10	44
DCBN (3 μM)	Protein adduct	37±7	72±12	62±12[a]	86
DCBN (30 μM)	Protein adduct	65±13	136±18	112±10[a]	82

[a]Not significantly different from 129/Sv mice; $p>0.05$.

[b]Not significantly different from B6 mice; $p>0.05$.

JPET Fast Forward. Published on November 10, 2003 as DOI: 10.1124/jpet.103.060301
This article has not been copyedited and formatted. The final version may differ from this version.

TABLE 4

Acetaminophen clearance in *Cyp2g1*-null and wild-type mice

Male, 3-month-old B6, 129/Sv, and *Cyp2g1*-null mice were treated at 9-10 A.M., after overnight fasting, with a single i.p. injection of AP (50 mg/ml) in 25% PEG at the indicated dose. Blood samples were collected at 15 min and 1, 2, 6, 8, and 12 hr after the injection for AP determination as described in Materials and Methods. Values presented are means ± S.D. AUC_{0-12} indicates the area under the time-concentration curve from 0 to 12 hr post AP administration.

Strain	Dose (mg/kg)	Body Weight (g)	AUC_{0-12} mg•h/ml
B6	400	27.4±2.4	2.5±0.4 (n=6)
	600	27.0±2.5	3.6±0.7 (n=7)
129/Sv	400	27.2±1.9	2.1±1.0 (n=5)
	600	28.6±3.9	4.3±0.5 (n=6)
Cyp2g1-null	400	31.4±6.4	2.0±0.3 (n=5)[a]
	600	26.0±2.6	3.6±1.2 (n=5)[b]

[a]There is no significant difference between *Cyp2g1*-null and 129/Sv mice; $p>0.05$.

[b]There is no significant difference between *Cyp2g1*-null mice and either of the corresponding wild-type groups; $p>0.05$.

JPET Fast Forward. Published on November 10, 2003 as DOI: 10.1124/jpet.103.060301
This article has not been copyedited and formatted. The final version may differ from this version.

TABLE 5

Acetaminophen toxicity in *Cyp2g1*-null and wild-type mice

Male, 3-month-old B6, 129/Sv, and *Cyp2g1*-null mice were treated at 9-10 A.M., after overnight fasting, with a single i.p. injection of AP (50 mg/ml) in 25% PEG at the indicated dose. Control groups received the vehicle only. Plasma ALT activity, hepatic total non-protein thiols, and histopathology of the nasal cavity were determined at 24 hr after injection for surviving animals as described in Materials and Methods. In control mice, the levels of plasma ALT were about 100 u/L, and levels of hepatic total non-protein thiol were about 6.0 μmol/g wet weight. Severity of lesions of the LNG was graded, with ++ representing moderate, + representing mild, +/- representing minimal, and - representing negative. The numbers of mice in each grade are shown.

Strain	Dose	24-hr Survival Rate[a]	Plasma ALT[b]	Hepatic NPT[b]	LNG Toxicity			
	mg/kg		*u/L*	*μmol/g wet weight*	++	+	+/-	-
B6	200	8/8	4000±3800 (n=8)	5.6±1.6 (n=8)	ND[c]			
	400	7/8	5500±2900 (n=7)	3.2±2.5 (n=7)	4	2		1
	600	3/8	3700±2600 (n=3)	2.7±1.8 (n=3)	2	1		
129/Sv	200	8/8	6300±3500 (n=8)	4.7±1.2 (n=8)	ND			
	400	7/8	5400±3200 (n=7)	2.8±1.8 (n=7)	5	2		
	600	2/8	3200, 1000 (n=2)	3.3, 3.0 (n=2)		1	1	
Cyp2g1-null	200	8/8	5200±2400 (n=8)	5.9±1.2 (n=8)	ND			
	400	8/8	3400±2900 (n=8)	4.4±1.5 (n=8)			1	7
	600	3/8	2300±500 (n=3)	3.1±0.7 (n=3)			2	1

[a]Number of mice survived over total number of mice tested.

[b]Means ± S.D. There is no significant difference between *Cyp2g1*-null mice and either of the corresponding wild-type groups.

[c]ND, not determined.

TABLE 6

CYP2A expression and activity in the LNG of *Cyp2g1*-null and wild-type mice

OM and LNG of female, 2-month-old B6, 129/Sv, and *Cyp2g1*-null mice (eight per group, pooled tissue) were used for the preparation of S9 fractions. Assays for coumarin 7-hydroxylation and AP-glutathione adduct formation were performed as described in Materials and Methods. An NADPH-regeneration system was used. Reaction mixtures contained 0.5 mM coumarin or AP and 0.5 (for OM) or 1.0 (for LNG) mg/ml S9 protein. Reactions were carried out for 10 to 30 min (for OM) or 2 hr (for LNG). Values presented are the averages of triplicate assays of the pooled samples.

Strain	Coumarin 7-Hydroxylation		AP-Glutathione Adduct Formation	
	pmol/min/mg protein		*pmol/min/mg protein*	
	LNG	OM	LNG	OM
B6	8	700	8	1740
129/Sv	14	2300	10	1780
Cyp2g1-null	5	2100	8	1650

JPET Fast Forward. Published on November 10, 2003 as DOI: 10.1124/jpet.103.060301
This article has not been copyedited and formatted. The final version may differ from this version.

Fig. 1

Zhuo et al.

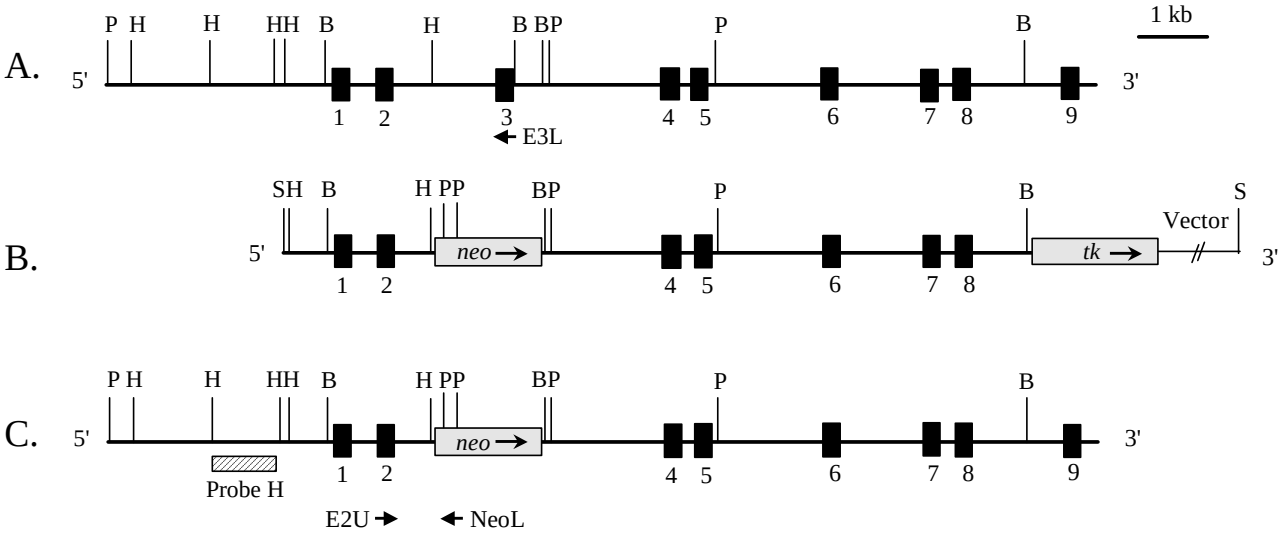

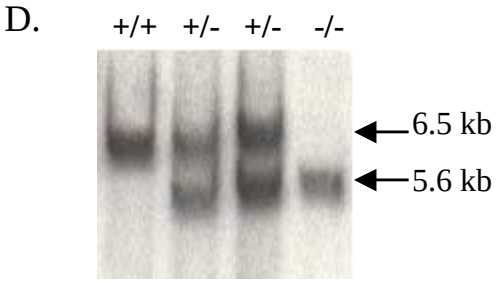

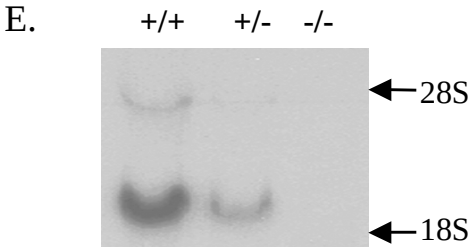

JPET Fast Forward. Published on November 10, 2003 as DOI: 10.1124/jpet.103.060301
This article has not been copyedited and formatted. The final version may differ from this version.

Fig. 2

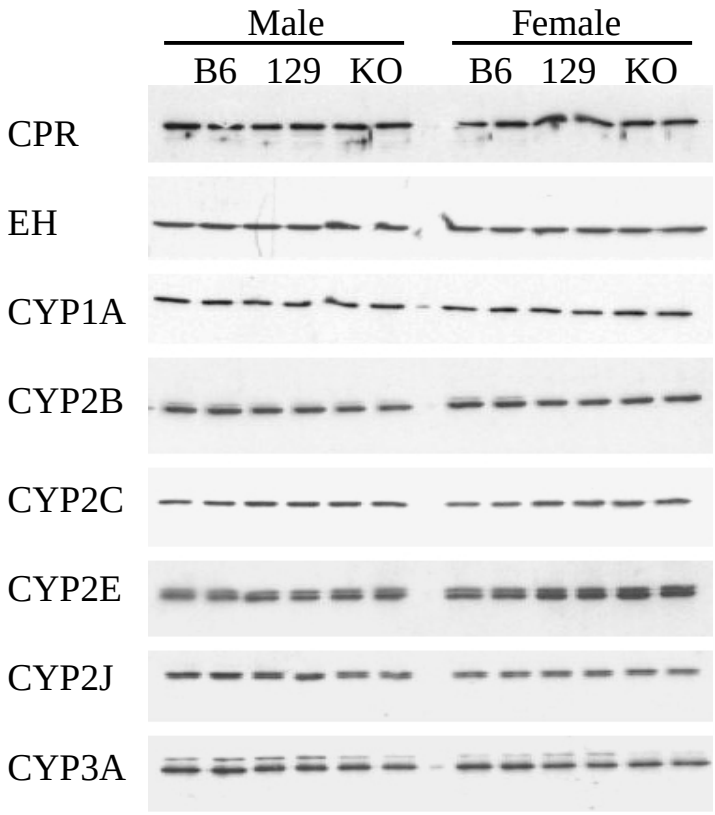

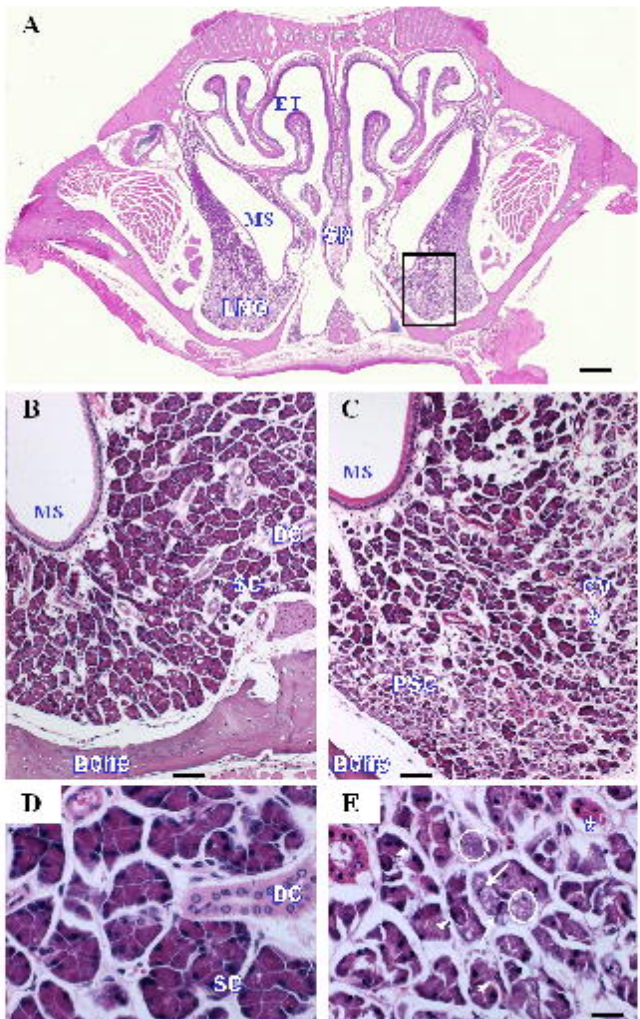
A
ET
MS
EP
LMC
B
MS
DC
SC
BONE
C
MS
CT
PSC
BONE
D
DC
SC
E

JPET Fast Forward. Published on November 10, 2003 as DOI: 10.1124/jpet.103.060301
This article has not been copyedited and formatted. The final version may differ from this version.

Fig. 4